Crystal Structure of the Cytomegalovirus DNA Polymerase Subunit UL44 in Complex with the C Terminus from the Catalytic Subunit DIFFERENCES IN STRUCTURE AND FUNCTION RELATIVE TO UNLIGANDED UL44

THE JOURNAL OF BIOLOGICAL CHEMISTRY VOL. 281, NO. 8, pp. 5224–5232, February 24, 2006

Crystal Structure of the Cytomegalovirus DNA Polymerase Subunit UL44 in Complex with the C Terminus from the Catalytic Subunit

*DIFFERENCES IN STRUCTURE AND FUNCTION RELATIVE TO UNLIGANDED UL44**

Received for publication, June 24, 2005, and in revised form, December 2, 2005 Published, JBC Papers in Press, December 20, 2005, DOI 10.1074/jbc.M506900200

Brent A. Appleton[‡§1], Justin Brooks[‡¶2], Arianna Loregian[‡3], David J. Filman[‡], Donald M. Coen[‡§], and James M. Hogle[‡§4]

From the [‡]Department of Biological Chemistry and Molecular Pharmacology, the [§]Committee on Virology, and the [¶]Summer Honors Undergraduate Research Program, Harvard Medical School, Boston, Massachusetts 02115

The human cytomegalovirus DNA polymerase is composed of a catalytic subunit, UL54, and an accessory protein, UL44, which has a structural fold similar to that of other processivity factors, including herpes simplex virus UL42 and homotrimeric sliding clamps such as proliferating cell nuclear antigen. Several specific residues in the C-terminal region of UL54 and in the "connector loop" of UL44 are required for the association of these proteins. Here, we describe the crystal structure of residues 1–290 of UL44 in complex with a peptide from the extreme C terminus of UL54, which explains this interaction at a molecular level. The UL54 peptide binds to structural elements similar to those used by UL42 and the sliding clamps to associate with their respective binding partners. However, the details of the interaction differ from those of other processivity factor-peptide complexes. Crucial residues include a three-residue hydrophobic "plug" from the UL54 peptide and Ile[135] of UL44, which forms a critical intramolecular hydrophobic anchor for interactions between the connector loop and the peptide. As was the case for the unliganded UL44 structure, the UL44-peptide complex forms a head-to-head dimer that could potentially form a C-shaped clamp on DNA. However, the peptide-bound structure displays subtle differences in the relative orientation of the two subdomains of the protein, resulting in a more open clamp, which we predicted would affect its association with DNA. Indeed, filter binding assays revealed that peptide-bound UL44 binds DNA with higher affinity. Thus, interaction with the catalytic subunit appears to affect both the structure and function of UL44.

The replication of DNA requires a number of multiprotein assemblies, including a DNA polymerase that synthesizes tens of thousands of nucleotides without dissociating from the primer-template. Most replicative DNA polymerases require not only catalytic subunits, but also accessory subunits known as processivity factors to remain tethered to the template during replication. The well characterized processivity factors known as sliding clamps, which include proliferating cell nuclear antigen (PCNA)[5] from eukaryotes and archaebacteria, β-subunits from prokaryotes, and gp45 from T4 and RB69 bacteriophage, display no intrinsic affinity for DNA. They tether their corresponding catalytic subunits to DNA after they are loaded onto DNA as toroidal homomultimers via clamp loader complexes in ATP-dependent processes (reviewed in Ref. 1).

Herpesviruses, including herpes simplex virus (HSV) and human cytomegalovirus (HCMV), encode a DNA polymerase consisting of two proteins that are essential for viral DNA replication (2–4). The DNA polymerase is composed of a 1242-residue catalytic protein, UL54 (5, 6), and a 433-residue accessory protein, UL44 or ICP36 (7). UL54, a member of the polymerase α family, displays DNA-dependent DNA polymerase and 3′–5′ exonuclease activities (8–10). UL44 is analogous to the processivity factor UL42 (11), as it binds double-stranded DNA, specifically interacts with UL54, and stimulates long chain DNA synthesis by UL54 (7, 12–15). Although not yet rigorously proven by template challenge experiments, UL44 is believed to serve as the processivity factor for the polymerase.

The crystal structure of residues 1–290 of UL44 (UL44ΔC290) (15) showed that UL44 has a fold remarkably similar to that of other processivity factors, including HSV UL42 (16) and monomers of the sliding clamps such as PCNA (17, 18), even though these proteins have no obvious sequence homology. Thus, each subunit of UL44, UL42, and PCNA consists of two topologically similar domains. The two domains share a central β-sheet and are connected by a long connector loop running lengthwise across the front face of the molecule.

UL44ΔC290 displays all known biochemical activities of full-length UL44 *in vitro* (12, 19). Both UL44 and UL42 bind directly to DNA with nanomolar affinity in a manner that does not require ATP hydrolysis or accessory proteins, and the binding interaction has no apparent sequence specificity (15, 20–23). UL44 forms a head-to-head C clamp-shaped homodimer (15, 24), in contrast to UL42, which is a monomer (11, 16, 25–27), and PCNA, which is a head-to-tail toroidal homotrimer (17, 18).

The extreme C terminus of the HSV catalytic subunit, UL30, binds to

* This work was supported in part by National Institutes of Health Grants AI19838 (to D. M. C.) and AI32480 (to J. M. H.). Use of the Argonne National Laboratory Structural Biology Center beamlines at the Advanced Photon Source was supported by United States Department of Energy, Office of Energy Research, under Contract W-31-109-ENG-38. The costs of publication of this article were defrayed in part by the payment of page charges. This article must therefore be hereby marked "*advertisement*" in accordance with 18 U.S.C. Section 1734 solely to indicate this fact.

The atomic coordinates and structure factors (code 1YYP) have been deposited in the Protein Data Bank, Research Collaboratory for Structural Bioinformatics, Rutgers University, New Brunswick, NJ (http://www.rcsb.org/).

[1] Present address: Dept. of Protein Engineering, Genentech, Inc., South San Francisco, CA 94080.

[2] Supported in part by Research Experiences for Undergraduates Grant DBI-0243489 from the National Science Foundation. Present address: Washington University Medical School, St. Louis, MO 63110.

[3] Present address: Dept. of Histology, Microbiology, and Medical Biotechnologies, Section of Microbiology, University of Padua, 35121 Padua, Italy.

[4] To whom correspondence should be addressed: Dept. of Biological Chemistry and Molecular Pharmacology, Bldg. C-2, Harvard Medical School, 240 Longwood Ave., Boston, MA 02115. Tel.: 617-432-3918; Fax: 617-432-4360; E-mail: jhogle@hms.harvard.edu.

[5] The abbreviations used are: PCNA, proliferating cell nuclear antigen; HSV, herpes simplex virus; HCMV, human cytomegalovirus.

the connector loop of UL42 in the crystal structure (16). As is the case with HSV UL42 (16, 28), residues in the connector loop of UL44 are required for interaction with its cognate catalytic subunit (19). Moreover, as is the case with HSV UL30, the C terminus of UL54 is both necessary and sufficient for binding to UL44 (12). This region displays some α-helical propensity in solution (29), although this tendency is less than that of corresponding peptides from the C terminus of HSV UL30 (30). However, unlike the HSV UL42-UL30 interaction, which is dominated by polar contacts (16, 31), the strength of the UL44-UL54 interaction appears most dependent upon several specific hydrophobic residues (12, 19).

The strength and specificity of the interaction between UL44 and a peptide corresponding to the C-terminal 22 residues of UL54 suggested that these two polypeptides might be crystallized as a complex. We have solved the structure of the complex of UL44ΔC290 with this C-terminal peptide from UL54. The structure provides an explanation for previous biochemical and molecular genetic studies (12, 19) that investigated the physical and functional association of the two subunits. The UL44-UL54 structure differs from other "processivity fold" structures in complex with their cognate binding partners. Like the free protein, the UL44-peptide complex forms a dimeric C-shaped clamp. However, the UL44 peptide structure has a more "open" conformation, which raised the possibility that this difference could affect DNA binding. This possibility has been confirmed experimentally, suggesting that interaction with UL54 affects both the structure and function of UL44.

MATERIALS AND METHODS

Protein Purification and Peptide Synthesis—Construction of the pD15-UL44ΔC290wt (where wt is wild-type) and pD15-UL44ΔC290(I135A) plasmids, which express residues 1–290 of UL44 as glutathione *S*-transferase fusion proteins, as well as the expression and purification of wild-type UL44ΔC290, UL44ΔC290(I135A), and selenomethionyl-UL44ΔC290 protein samples were described previously (12, 15, 19). Peptides corresponding to the C-terminal 22 residues of HCMV UL54 and the C-terminal 36 residues of HSV UL30 were synthesized and purified in the Biopolymers Laboratory of the Department of Biological Chemistry and Molecular Pharmacology and resuspended in water as described (12).

Crystallization and Structure Solution—Selenomethionyl-UL44ΔC290 was concentrated to ~125 μM in 20 mM Tris-HCl (pH 7.5), 500 mM sodium chloride, 20% glycerol, 0.1 mM EDTA, and 2 mM dithiothreitol; stored at −80 °C; and thawed from frozen stocks as described (15). One μl each of UL44ΔC290, UL54 peptide (~300 μM in water), and well solution were combined and crystallized by vapor diffusion at 22 °C in hanging drops. Similar orthorhombic crystal forms were found using a well solution composed of either 2 M ammonium sulfate, 100 mM phosphate-citrate (pH 4.2), and 10 mM dithiothreitol or 2.5 M sodium chloride, 100 mM sodium acetate (pH 4.5), 200 mM lithium sulfate, and 10 mM dithiothreitol. For structure determination, the well solution containing ammonium sulfate was used. Crystals reached ~250 × 250 × 250 μm in 5–7 days. The drop solution was supplemented with a cryosolution of 40% ethylene glycol plus well solution until the final concentration reached ~20–25% ethylene glycol. Crystals were flash-frozen in liquid nitrogen.

Experimental phases were obtained from a multiwavelength anomalous dispersion experiment on a single crystal of selenomethionyl-UL44ΔC290 complexed with the C-terminal UL54 peptide using a four-wavelength data set collected at beamline 19-ID at the Advanced Photon Source (Argonne, IL) (see Table 1). Images were processed with DENZO and merged with SCALEPACK (32). Initial phases were determined using SOLVE (33), which located four of five possible selenium sites and reported a figure of merit of 0.65. Density modification was performed with RESOLVE (34), resulting in readily interpretable electron density maps. Atomic models were built using XtalView (35) and refined by the maximum likelihood method with REFMAC Version 5.1 (36), maintaining experimental phases as restraints throughout refinement. The anisotropic motion of the protein was modeled using TLS (translation/libration/screw motion) refinement in REFMAC. Figures were produced using PyMOL (available at www.pymol.org) or MolScript (38) with Raster3D (39).

Filter Binding Assay—Filter binding assays of DNA binding were performed as described (15) with minor modifications. Briefly, increasing amounts of wild-type UL44ΔC290 or UL44ΔC290(I135A) were incubated with 1 fmol of radiolabeled double-stranded 30-bp DNA in the absence or presence of 50 μM peptide corresponding to the C-terminal 22 residues of HCMV UL54 or the C-terminal 36 residues of HSV UL30.

RESULTS AND DISCUSSION

Structure Determination—The complex of UL44ΔC290 and a 22-residue peptide corresponding to the C terminus of UL54 (residues 1221–1242) was crystallized in space group $C222_1$ with unit cell dimensions of $a = 91.8$, $b = 127.6$, and $c = 66.0$ Å and with one molecule/asymmetric unit. The structure of the complex was determined by multiwavelength anomalous dispersion of one selenomethionyl crystal using SOLVE (33) and was subsequently refined to 2.5-Å resolution (Table 1). Three regions of the UL44ΔC290 molecule that are disordered in the uncomplexed structure (15) remain disordered in the complex. These regions are the first eight residues of the N terminus, the last 19 residues of the C terminus, and an internal loop composed of residues 163–176. All of the 22-residue UL54 peptide could be positioned unambiguously in the electron density maps, except for the first two residues of the N terminus. The atomic model is reported with an R_{cryst} and R_{free} of 0.195 and 0.227, respectively.

General Features of the Structure—As observed in the unliganded structure (15), UL44ΔC290 adopts a fold similar to those of UL42 (16) and PCNA (17, 18) when bound to the peptide (Fig. 1). The UL44ΔC290 structure is composed of two topologically similar domains (an N-terminal domain, residues 9–128; and a C-terminal domain, residues 143–271) linked covalently by an interdomain connector loop (residues 129–142). The β-strands at the edge of each domain are hydrogen-bonded with one another to create a central, nine-stranded β-sheet. Each UL44 molecule can be defined to have a "front" and "back" face. The connector loop crosses the front face of the central β-sheet, creating a potential binding site for the peptide on each side of the loop. The back face of the central β-sheet of UL44ΔC290 is decorated by four helices that include several basic residues, previously hypothesized to be involved in binding to the sugar phosphate backbone of DNA (15). The N- and C-terminal domains each have an additional four- or five-stranded β-sheet at the distal end of the molecule that lies roughly perpendicular to the large central β-sheet and that participates in forming multimers of UL44 (see below). The UL54 peptide begins with an extended conformation of its N-terminal six residues before forming a short helix (residues 1228–1233), followed by a β-strand (residues 1235–1237) and a single helical turn (residues 1239–1241) (Fig. 1). (Residue numbers from 1221 to 1242 correspond to the UL54 peptide, whereas all other numbers correspond to UL44.) Thus, this UL54 peptide is less α-helical than the analogous peptide derived from the HSV catalytic subunit, UL30 (16). This observation is consistent with circular dichroism studies demonstrating that the C-terminal peptide of HCMV UL54 is less α-helical in solution than similar peptides from HSV UL30 (29, 30). The UL54 peptide makes several interactions with regions on the front face of UL44, which are detailed below. Altogether, peptide binding by UL44 buries ~1400 $Å^2$ of

TABLE 1

Data collection and refinement statistics

r.m.s.d., root mean square deviation.

Data collection				
Space group	$C222_1$			
Unit cell (Å)	$a = 91.79, b = 127.6, c = 65.98$			
	Peak	**Inflection**	**Low energy**	**High energy**
Wavelength (Å)	0.9793	0.9794	1.008	0.9537
Resolution (Å)	30 to 2.5	30 to 2.5	30 to 2.5	30 to 2.5
Unique reflections	13,802	13,878	13,756	14,162
Total measurements	196,044	198,189	195,533	196,828
Completeness (%)[a]	99.9 (100.0)	99.9 (100.0)	99.9 (100.0)	99.9 (100.0)
R_{sym} (%)[a,b]	5.8 (20.3)	5.3 (22.9)	4.1 (15.7)	4.9 (20.7)
$\langle I\rangle/\langle\sigma(I)\rangle$[a]	44.8 (13.7)	49.6 (13.0)	68.3 (20.3)	54.2 (14.6)
Refinement				
Resolution (Å)[a]	30 to 2.5 (2.63 to 2.5)			
R_{cryst}[c]	0.195 (0.203)			
R_{free}[c]	0.227 (0.304)			
Non-hydrogen atoms				
Protein	2107			
Solvent	80			
Average *B*-factor (Å^2)	32.7			
r.m.s.d. bonds (Å)	0.012			
r.m.s.d. angles	1.9°			
Ramachandran plot (%)[d]	90.0/9.1/0.8/0			

[a] Values in parentheses refer to data in the highest resolution shell.
[b] $R_{sym} = \Sigma_{hkl}|I_{hkl} - \langle I_{hkl}\rangle|/\Sigma_{hkl}\langle I_{hkl}\rangle$, where $\langle I_{hkl}\rangle$ is the mean intensity of symmetry-related observations of a unique reflection.
[c] $R_{cryst} = R_{free} = \Sigma_{hkl}|F_o - F_c|/\Sigma_{hkl}|F_o|$, where R_{free} represents 5% of the data selected randomly.
[d] Values represent the percentage of residues in the most favored, additionally allowed, generously allowed, and disallowed regions, respectively, of the Ramachandran plot as determined by PROCHECK (37).

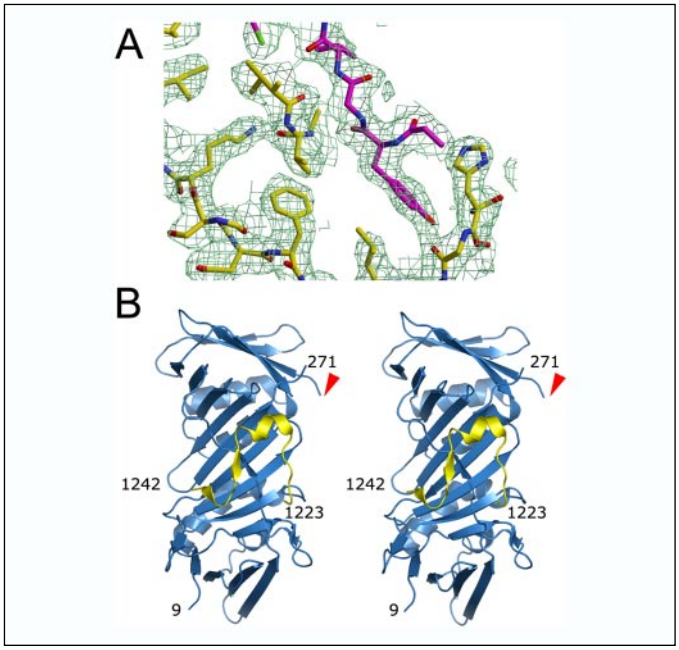

FIGURE 1. **Structure of the UL44ΔC290-UL54 peptide complex.** *A*, cross-section of the refined model positioned in the 2.5-Å solvent-flattened experimental electron density map, which is contoured at 1σ. The carbon atoms in the UL44ΔC290 and UL54 atomic models are colored *yellow* and *magenta*, respectively. Oxygen, nitrogen, and sulfur atoms are colored *red*, *blue*, and *green*, respectively. *B*, stereoscopic ribbon representation of the UL44ΔC290-UL54 peptide complex (*blue* and *yellow*, respectively). The peptide binds to the front face of the central β-sheet, interacting with the connector loop and adjacent regions. The last ordered residue at the N and C termini of each polypeptide is indicated. The *red arrowheads* indicate the approximate positions of a 16-residue disordered loop.

solvent-accessible surface and exhibits a shape complementarity of 0.75 (the shape complementarity statistic as defined by Lawrence and Colman (40)).

Molecular Details of the UL44-UL54 Interaction—The UL54 peptide makes two major sets of interactions with UL44. One involves a hydrogen-bonding network between the middle portion of the peptide (residues 1234–1238) and, lying along its "right" edge, the central part of the connector loop (residues 133–137) (Fig. 2*A*). This includes four main chain-to-main chain hydrogen bonds, which participate in an antiparallel β-sheet between the connector loop and the peptide. Additional contacts with the peptide come from UL44 side chains. Thus, the ϵ-oxygen and ϵ-nitrogen of Gln^{133} form hydrogen bonds with the main chain nitrogen and oxygen, respectively, of Leu^{1225}. Additionally, the side chain of Asp^{134} forms a salt bridge with Lys^{1237} of the peptide and coordinates two water molecules with the main chain of the peptide at Leu^{1225} and Leu^{1227} (data not shown). The central portion of the connector loop is further stabilized by three intramolecular hydrogen bonds between the side chains of Gln^{51} and Lys^{60}, which extend upward from the central β-sheet and bind to the main chain of the connector loop (thus extending the β-sheet hydrogen-bonding pattern along its right edge) at Asp^{134} and Val^{136}, respectively (Fig. 2*A*). Although the side chain of Ile^{135} forms some van der Waals interactions with the peptide, including the sulfur of Cys^{1241} and C-β of Ala^{1238}, these interactions are less extensive than the hydrophobic interactions that Ile^{135} makes with other side chains of UL44. Thus, the side chain of Ile^{135} is positioned as a hydrophobic "anchor" underneath the hydrogen-bonding network, where it makes favorable van der Waals contacts with several important residues from the central β-sheet of UL44, including Val^{41}, Ile^{49}, and the aliphatic portions of Gln^{51} and Lys^{60}.

The second set of interactions involves the packing of a hydrophobic "plug" into a crevice along the central β-sheet of UL44 (Fig. 2, *B* and *C*). This crevice is formed principally by side chains of several residues from the central β-sheet and is located just to the right of the connector loop at the boundary between the N- and C-terminal domains. The hydrophobic plug of the UL54 peptide is composed of three side chains (Leu^{1227}, Phe^{1231}, and Tyr^{1234}). All three side chains extend toward the surface of UL44 from a segment of the main chain (residues 1228–1234) that assumes a roughly helical conformation, despite the presence of proline residues at positions 1229 and 1233. Leu^{1227} and Phe^{1231} pack into pockets formed by Val^{136} of the UL44 connector loop and several residues from the central β-sheet, including Val^{53}, Val^{58}, Leu^{251}, and Phe^{266}, as well as the aliphatic portions of Thr^{268} and Lys^{60}. Tyr^{1234} of

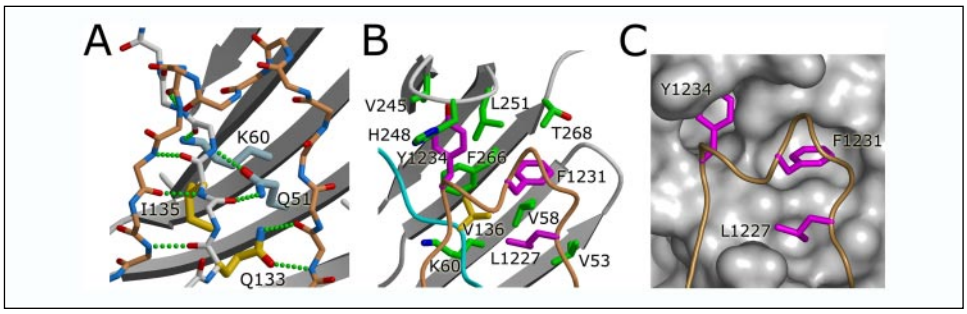

FIGURE 2. **Molecular details of the UL44-UL54 interface.** *A*, the connector loop of UL44 (*white*) and the UL54 peptide (*brown*) are joined by an extensive network of hydrogen bonds (*green dots*). Four intermolecular hydrogen bonds are formed between main chain atoms of the connector loop (residues 133–137) and the peptide (residues 1234–1238). Additional hydrogen bonds are observed between the side chain of Gln^{133} (*yellow*) of UL44 and the main chain of the peptide and between the side chains of Gln^{51} and Lys^{60} (*light blue*) of UL44 and the main chain of the connector loop. Ile^{135} (*yellow*) of UL44 forms a critical hydrophobic anchor below the hydrogen-bonding network. For clarity, only the side chains of Gln^{51}, Lys^{60}, Gln^{133}, and Ile^{135} are shown. *B*, Leu^{1227}, Phe^{1231}, and Tyr^{1234} (*magenta*) are part of a hydrophobic plug that packs against a hydrophobic crevice composed of Val^{136} (*yellow*) from the connector loop (*cyan*) as well as hydrophobic and aliphatic side chains (*green*) from the central β-sheet of UL44. *C*, the molecular surface of UL44 reveals pockets that accommodate the three-residue hydrophobic plug of UL54.

the peptide is partially buried between Val^{245}, Leu^{251}, His^{248}, and Phe^{266} of UL44 and Pro^{1233} of the peptide. The hydroxyl oxygen of Tyr^{1234} also forms a hydrogen bond with the main chain nitrogen of His^{248}.

Relation of the Observed Interactions in the UL44 Peptide Structure to the Results of Molecular Genetic and Biochemical Experiments—Prior to this study, experiments were initiated to identify which residues are crucial for the interaction between the two HCMV DNA polymerase subunits (12, 19). Based on analogous studies of HSV DNA polymerase subunits (16, 28, 31), a series of mutant constructs were engineered with individual alanine substitutions in residues 129–140 of the HCMV UL44 connector loop (19) or in the C-terminal 22 residues of HCMV UL54 (12). Each mutation was tested for its effect on the association of UL44 and UL54 and on the ability of UL44 to stimulate long chain DNA synthesis by UL54. Several UL44 mutants were also tested for their affinity for the peptide ligand that is present in the crystal structure, which corresponds to the C terminus of UL54.

In the connector loop, only alanine substitutions at UL44 residues 133–136 reduce the physical and functional interactions of UL44 with full-length UL54 and with its C terminus (19). Of these, only one substitution (I135A) completely disrupts this interaction. As noted above, the bulky side chain of Ile^{135} makes extensive intramolecular interactions to form a hydrophobic anchor beneath the connector loop, along with some less extensive interactions with the peptide. Indeed, even though Ile^{135} contacts the sulfur group of Cys^{1241}, an alanine substitution at residue 1241 has no impact. The atomic model of the complex with the peptide suggests why the Ile^{135} side chain is so critical. Removal of that side chain would leave a highly unfavorable hole in a buried hydrophobic core, implying that the I135A mutant cannot form a stable complex.

Although the central portion of the connector loop (residues 133–137) is tightly associated with residues of the underlying β-sheet and makes numerous contacts, the flanking sequences (positions 129–132 and 138–140) do not participate in sequence-specific interactions. These structural observations help to explain the results of our molecular genetic and biochemical studies, wherein single alanine substitutions at Gln^{133}, Asp^{134}, and Val^{136} partially reduce HCMV UL44-UL54 binding, and replacement of Ile^{135} abolishes binding, whereas alanine substitutions in the flanking sequences of the connector loop have no effect.

In a parallel study, we examined mutations in the C-terminal region of UL54 (12). Alanine substitution at Leu^{1227} or Phe^{1231} abolishes detectable binding between UL44 and UL54. A partial impairment is also observed with substitution at Arg^{1224}, His^{1226}, or Tyr^{1234} or deletion of the two C-terminal cysteines at residues 1241 and 1242. The effects of most of these mutations are explained by interactions observed in the crystal structure. Three of these substitutions, including the two with the most severe defects, affect hydrophobic residues, *viz.* Leu^{1227}, Phe^{1231}, and Tyr^{1234}, which form the hydrophobic plug (Fig. 2, *B* and *C*). Substitution at Arg^{1224} or His^{1226} also slightly affect binding, but the reason is less clear, as these two residues do not make noticeable interactions with UL44 in the structure. Deletion of the two C-terminal cysteines also reduces interactions of either full-length UL54 or the UL54 C-terminal peptide with UL44, reducing the affinity of the peptide for UL44 by ~10-fold (12). In the crystal structure, the C-terminal four residues of UL54 are positioned adjacent to the connector loop on the "left" side opposite the hydrophobic crevice (Fig. 2, *B* and *C*). These four residues help to bury a hydrophobic patch that includes the side chains of Ile^{135}, Leu^{43}, and Ile^{49}, which would be solvent-exposed in their absence. In addition, we observed a hydrogen bond between the terminal carboxylate group of the peptide and the side chain of Thr^{45}. Shortening the peptide by two residues would have positioned its charged carboxylate in a much less favorable environment, near the aliphatic side chains of Leu^{43} and Pro^{77}. Thus, the UL44-UL54 structure provides a clear explanation for the effects of most of the alanine substitutions and helps to explain why alanine substitutions at hydrophobic residues have the most dramatic effects in HCMV (12, 19).

Comparison with the HSV UL42-UL30 Peptide Structure—The HCMV UL44-UL54 peptide structure is significantly different from the structure of HSV UL42 in complex with a peptide that corresponds to the C-terminal 36 residues of UL30 (16). In the HSV UL42-UL30 complex, the peptide adopts an α-β-α fold (Fig. 3). As in the HCMV complex, the middle of the HSV peptide forms an antiparallel β-β interaction with the middle of the interdomain connector loop. However, these contacts are probably less important in HSV. In HSV, most of the buried surface and critical contacts involve the C-terminal 15-residue helix of the UL30 peptide, which has no structural counterpart in HCMV. It binds within an extended groove to the left of the β-β interactions (Fig. 3*A*). Isothermal titration calorimetry experiments are consistent with structural observations. They have demonstrated the importance of this helix in HSV, showing that a peptide corresponding to the C-terminal 18 residues of HSV UL30 binds to UL42 nearly as well as the 36-residue peptide does and that three residues from the terminal helix (His^{1228}, Arg^{1229}, and Phe^{1231}) are required for binding (31). All three residues make obvious contacts in the crystal structure (Fig. 3*A*). Note that, unlike HCMV, several of the key sequence-specific interactions in HSV are polar.

A closer structural parallel between HSV and HCMV can be drawn involving the helix that precedes the antiparallel β-β interac-

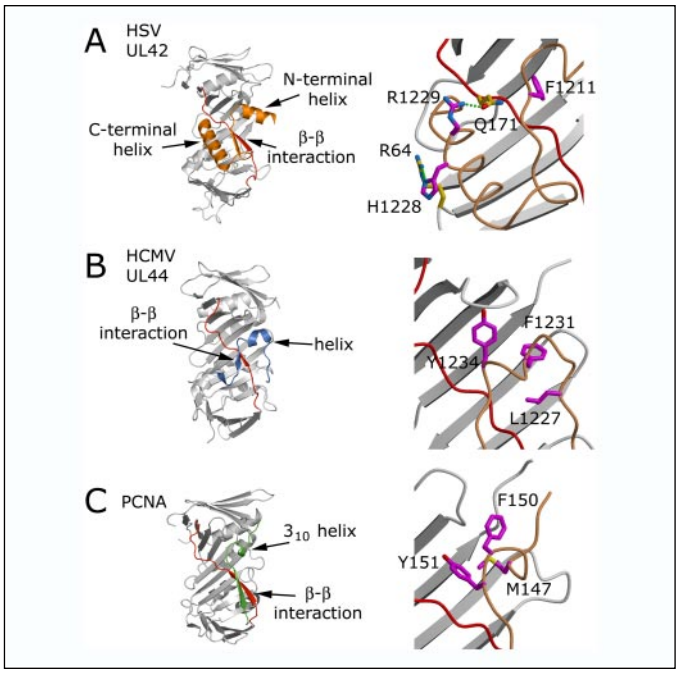

FIGURE 3. **Comparison of the processivity factor-peptide structures of HSV UL42, HCMV UL44, and human PCNA.** *A*, the association of HSV UL42 (Protein Data Bank code 1DML) with the UL30 peptide (*orange*) is primarily stabilized by interactions between the C-terminal helix of the peptide and a groove on the left side of the connector loop (*red* in each panel). His[1228] and Arg[1229] from the C-terminal helix of the peptide are hydrogen-bonded to Arg[64] and Gln[171], respectively, of UL42. *B*, in contrast, the HCMV UL54 peptide (*blue*) makes significant interactions with UL44 on the right side of the connector loop. This interaction depends largely on three hydrophobic residues from the peptide that bind to a hydrophobic crevice on UL44. The side chains of Leu[1227] and Phe[1231] of UL54 are required for the association with UL44. Although the HSV UL30 peptide has an aromatic residue (Phe[1211]) that packs into an analogous crevice on UL42 (see *inset* in *A*), this interaction is not essential. *C*, like UL44, PCNA (Protein Data Bank code 1AXC) contains a hydrophobic crevice on the right side of the connector loop that binds to a peptide from its respective binding partner, p21$^{WAF1/CIP1}$ (*green*). Similar to the UL54 peptide, the p21$^{WAF1/CIP1}$ peptide buries three hydrophobic residues in the crevice. The connector loop from each processivity factor forms an antiparallel β-sheet with its respective peptide. In each *inset*, the processivity factor is *gray*; the connector loop is *red*; and the peptide backbone is *tan*.

tion in the sequence of the bound C-terminal peptide. Such a helix is present in both HCMV UL54 and HSV UL30 (and also in some complexes with PCNA; see below). In each case, this helix lies to the upper right of the β-β region, and its principal interactions with the processivity factor involve the side chains of hydrophobic residues from the C-terminal end of the helix, binding to a positionally conserved hydrophobic "crevice" on the surface of the processivity factor. In this analogy, Phe[1211] and Leu[1206] of HSV might be functionally similar to Phe[1231] and Tyr[1234] of HCMV (Fig. 3), although very different in detail. In HSV, the helix, a true α-helix, makes contact with UL42 only at its C-terminal end (The remainder of the helix projects away from the UL42 surface.) Although the existence of these hydrophobic side chain interactions in HSV might offer clues to evolutionary relationships, they are much less important for complex formation than the ones in HCMV, as they can be deleted without affecting binding affinity (31). In contrast, in HCMV, an overall helical conformation of the main chain is maintained by main chain hydrogen bonding, but it is interrupted by the presence of prolines; the large hydrophobic side chains are distributed differently on the surface (Fig. 3); and mutating any of them to alanine has a significant impact on the binding of the HCMV UL54 peptide to UL44 (12).

The Sliding Clamps Interact with Their Binding Partners via a Hydrophobic Crevice—Even though sliding clamps were originally described as processivity factors for replicative DNA polymerases, subsequent studies have demonstrated their remarkable capacity to interact with other proteins involved in DNA replication as well as proteins involved in cell cycle regulation, DNA repair, and DNA recombination (reviewed in Refs. 41 and 42). Many of the proteins that bind to PCNA encode an eight-residue PCNA-interacting protein box described as Q*xxhxxaa* (where *x*, *h*, and *a* represent any residue, large hydrophobic residues (Met/Leu/Ile), and aromatic residues (Phe/Tyr/Trp), respectively). Several structures of sliding clamps have been solved in complex with peptides or full-length proteins from these binding partners, including the p21$^{WAF1/CIP1}$ cell cycle inhibitor (17), the Fen-1 endonuclease (43–45), the clamp loader complex (46, 47), and the DNA polymerase (44, 48). In each complex, the binding partner binds specifically to the front face of the clamp, where hydrophobic interactions are formed between the *hxxaa* motif and a pocket on the right side of the connector loop. (Fig. 3*C* shows a representative example of the PCNA-p21$^{WAF1/CIP1}$ structure.) In general, the first, fourth, and fifth residues of the *hxxaa* motif lie packed together on one face of a 3_{10} helix that is conserved among the PCNA-protein complexes. These side chains are involved in hydrophobic interactions with the pocket, which is formed by side chains from the connector loop and β-strands at the interdomain boundary of the clamp. In contrast, interactions involving residues outside of the *hxxaa* motif are not as well conserved. For example, the canonical PCNA-interacting protein box begins with a glutamine residue (41, 42), which forms hydrogen bonds with the last β-strand of the clamp, but this interaction is not observed in the clamp loader structures (46, 47). In addition, only the p21$^{WAF1/CIP1}$ peptide (17) and full-length Fen-1 (45) structures have an extended β-β interaction with the interdomain connector loop analogous to UL44 and UL42 (Fig. 3). Notably, however, the position of the hydrophobic pocket to which the *hxxaa* motif binds is conserved among the sliding clamp structures and is similar in location to the crevice found in UL44.

A similarly positioned hydrophobic binding site is also seen in yet another multimeric processivity factor, the β-subunit from *Escherichia coli* (49). The β-subunit is composed of three subdomains that are similar in topology to the N- and C-terminal domains of UL44 and PCNA. The β-subunit contains a hydrophobic binding site that is in a position analogous to the crevice on UL44 and PCNA. This was demonstrated in structures of the β-subunit bound to the δ-subunit of the clamp loader complex (50) and the translesion DNA polymerase, polymerase IV (51, 52).

It is noteworthy that the position of the hydrophobic crevice is conserved among PCNA, UL44, UL42, and the β-subunit. In each case, the bound peptide that contacts the hydrophobic crevice assumes a roughly helical conformation, with the important hydrophobic side chains clustered on the face of the helix facing the crevice (Fig. 3). Furthermore, in each case, the hydrophobic crevice is formed principally by hydrophobic side chains (and the aliphatic portions of polar side chains) projecting outward from the β-sheet of the processivity factor and laterally from the connector loop. However, the molecular details that define the interactions with their binding partners are not identical. Like the p21$^{WAF1/CIP1}$ peptide, the HCMV UL54 peptide relies on a plug composed of one hydrophobic (Leu[1227]) and two aromatic (Phe[1231] and Tyr[1234]) residues that are buried in the hydrophobic crevice. However, these three residues do not participate in forming the *hxxaa* motif or the ideal 3_{10} helix that is conserved among the PCNA-protein complexes. When the structurally equivalent residues of the HCMV UL44-UL54 peptide and PCNA-p21$^{WAF1/CIP1}$ peptide complexes are superimposed, both similarities and differences are observed (Fig. 4). Thus, Phe[1231] and Tyr[1234] of HCMV UL54 occupy positions that are structurally analogous to the binding sites of Met[147] and Tyr[151] of the

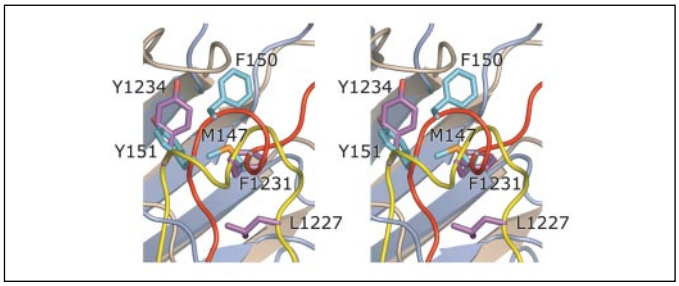

FIGURE 4. **Comparison of hydrophobic interactions in the UL44-UL54 and PCNA-p21$^{WAF1/CIP1}$ structures shown in stereo.** The hydrophobic crevices of UL44 (*tan*) and PCNA (*light blue*) are in similar locations adjacent to the connector loop. However, the three hydrophobic residues of the p21$^{WAF1/CIP1}$ (backbone (*red*) and side chains (*cyan*)) and UL54 (backbone (*yellow*) and side chains (*magenta*)) peptides, which are critical for binding, are not structurally similar to one another.

p21$^{WAF1/CIP1}$ peptide. However, HCMV Leu^{1227} is bound in a spot that has no counterpart in the PCNA complex, and its main chain atoms do not participate in forming the helical arrangement that is common to all of the bound peptides. It should also be noted that, although peptide binding to the hydrophobic crevice has been structurally conserved among the multimeric processivity factors, it plays a more limited role in peptide binding to HSV UL42, where only a single aromatic side chain from the peptide is buried in the pocket. Both the similarities in folding topology and similarities in peptide binding may eventually be relevant to working out the evolutionary relationships between UL44, UL42, and PCNA.

The existence of an independent binding site on each subunit of HCMV UL44 and the sliding clamps is intriguing because it creates the potential for a number of different proteins to be bound simultaneously. For example, during DNA lesion repair, it has been hypothesized that sliding clamps function as "tool belts" in which each binding site can accommodate a different repair polymerase (53). Perhaps HCMV UL44 could similarly interact with proteins that include a domain that resembles the plug observed in UL54. Thus, if UL44 functions as a homodimeric processivity factor in complex with one copy of UL54, the second binding site could accommodate additional viral or cellular factors needed for DNA replication. Alternatively, in the absence of UL54, UL44 could bind other proteins and function as a mobile platform on DNA by sliding nonspecifically via electrostatic interactions formed between basic residues of the back face of the protein and the phosphate backbone of DNA.

The HCMV UL44-UL54 Interaction as a Drug Target—Currently available drugs against HCMV, which target the polymerase activity of UL54, are hampered by problems of pharmacokinetics, resistance, and toxicity (54). The interaction between UL44 and UL54 would make an attractive drug target because it is specific and differs in important details from the PCNA-binding partner interactions and because both proteins are essential for viral replication (3, 4, 55). The interaction is known to be inhibited by peptides corresponding to the C-terminal 22 residues of UL54 (29), and the interaction has been shown to be sensitive to amino acid substitutions in either of the two subunits (12, 19). A similar strategy has been utilized for their counterparts in HSV (30, 31, 56), and small molecules have been identified that block both the HSV UL42-UL30 interaction *in vitro* and viral replication (57). In HCMV, the interaction appears even more amenable to small molecule inhibitors given the discrete hydrophobic crevice of UL44. Indeed, small molecules have been identified that block the HCMV UL44-UL54 peptide interaction, the UL44-UL54 interaction, and long chain DNA synthesis *in vitro* and that interfere with viral replication in cell-based assays (58). Details of the UL44 complex with the C terminus of UL54 may provide a basis for structure-based drug design.

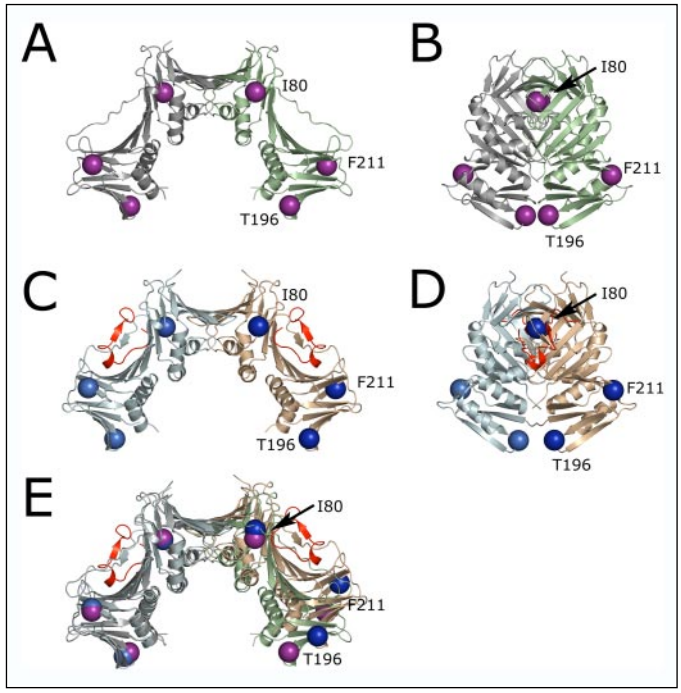

FIGURE 5. **UL44 displays a more open conformation in the complex.** The cavity of the C-shaped clamp opens from ~28 Å (*A* and *B*; without peptide) to 40 Å (*C* and *D*) upon peptide binding. Although this change may be the result of crystal-packing forces, it may also reflect differences in the conformation of UL44 when UL54 is present (see "Results and Discussion"). Large spheres (proxy atoms listed in Table 2) are included as landmarks to make molecular motions (pseudo-torsions) more obvious. *A* and *C* are orthogonal to *B* and *D*. The leftmost monomer from each head-to-head dimer has been superimposed in *E* so that positional differences in the rightmost monomers are emphasized.

Differences in Conformation of the C-shaped Clamp in the Unliganded Versus Liganded State—We reported previously that the unliganded structure of UL44ΔC290 forms a C clamp-shaped homodimer (15), and it was verified that UL44ΔC290 dimerizes in solution (15, 24). At that time, we presented a model in which the central cavity of the UL44 dimer could accommodate double-stranded DNA, and the basic back face of UL44 would make favorable electrostatic interactions with the phosphate backbone (15). These interactions would permit UL44 to tether the polymerase to the template, but also slide during replication. Consistent with this model, UL44ΔC290 also assembled as a C clamp-shaped homodimer when bound to the UL54 peptide (Fig. 5). In both the unliganded and peptide-bound crystal structures of UL44ΔC290 (space groups $P6_122$ and $C222_1$, respectively), this head-to-head dimerization involves the short β-sheet at the N-terminal end of the molecule. Two copies of this sheet, related by an intermolecular 2-fold axis, are hydrogen-bonded to form an extended sheet in each dimer. In both crystal forms, this intermolecular 2-fold axis happens to coincide with a crystallographic 2-fold axis, resulting in a crystal form with one molecule/asymmetric unit. Stabilization of the homodimer interface also involves van der Waals interactions between several hydrophobic side chains. Alanine substitution of a number of these residues disrupts both dimerization in solution and DNA binding (15). When the region around the homodimer interface is compared in the two crystal structures, few appreciable differences are seen (see below). This finding confirms that the homodimer interface is stable and supports the idea that the C-shaped clamp is biologically relevant, rather than an artifact of crystallization. In both crystal structures, with and without bound peptide, model-based statistics (buried surface area and shape complementarity) (Table 2) suggest that the monomers bind tightly to one another in head-to-head dimerization.

TABLE 2

Calculations from the unliganded and liganded UL44 structures

NA, not applicable.

Binding contacts between molecules	Interface				
	Head-to-head dimer interface	Tail-to-tail crystallographic interface	UL44-UL54 peptide		
Unliganded UL44 structure ($P6_122$)[a]					
Observed	Yes	No	NA		
Shape complementarity[b]	0.79	NA	NA		
Buried surface (Å^2)	1100	NA	NA		
UL44-UL54 peptide structure ($C222_1$)					
Observed	Yes	Yes	Yes		
Shape complementarity[b]	0.78	0.66	0.75		
Buried surface (Å^2)	1000	750	1400		
Individual C-α atoms used as proxies to illustrate relative motion of monomers	**Within individual monomers**			**Between monomers**	
Distances (Å)					
Residues[c]	Ile^{80}–Thr^{196}	Thr^{196}–Phe^{211}	Phe^{211}–Ile^{80}	Thr^{196}–Ile$^{80\prime}$	Thr^{196}–Thr$^{196\prime}$
UL44 structure	38	26	39	59	**52**
UL44-UL54 structure	40	25	38	60	**63**
Pseudo-torsions					
Residues[c]	Phe^{211}–Ile^{80}–Ile$^{80\prime}$–Phe$^{211\prime}$		Thr^{196}–Ile^{80}–Ile$^{80\prime}$–Thr$^{196\prime}$	Thr^{196}–Phe^{211}–Ile^{80}–Ile$^{80\prime}$	
UL44 structure	**92°**		**13°**	−84°	
UL44-UL54 structure	**104°**		**21°**	−86°	

[a] As previously reported for the unliganded UL44 structure (15).

[b] Shape complementarity is defined by the shape complementarity statistic (40).

[c] Residues denoted with primes belong to the symmetry-related monomer lying across the head-to-head dimer interface. Ile^{80} is a residue from one edge of the central β-sheet, adjacent to the amino (head-to-head) dimer contact area. Phe^{211} is a residue from the outer edge of the central β-sheet, adjacent to the carboxyl (tail-to-tail) dimer contact area. Thr^{196} belongs to the central β-sheet at the C-terminal end, is close to the tail-to-tail contact site, and faces the putative DNA-binding cavity. Observe that even when the symmetry-related Ile$^{80\prime}$ is included, the monomer is a good approximation to a single rigid body. In contrast, when the Ile^{80}–Ile$^{80\prime}$ axis is used as pivot, the pseudo-torsion between symmetry-related copies of the central sheet varies by 8–12°, which is largely responsible for the 12-Å change in the width of the central cavity of the dimer.

Despite these structural similarities at the head-to-head homodimer interface, the C-shaped clamp exhibits a surprisingly large increase in the diameter of the cavity from ~28 to 40 Å (Fig. 5). The program DYNDOM (59), which is designed to detect domain motions automatically, confirmed that it is valid to regard the dimer as being composed of two distinct domains. Root mean square differences between main chain atoms of the superimposed dimers (3.00 Å) are large compared with the differences within monomers (1.44 Å), although no specific mechanical hinge points can be identified in the dimer to explain the motion. Consistent with this idea, the differences between structures increase gradually as larger and larger groups of atoms are considered (data not shown). The opening and closing motion of the UL44 dimer can be understood as analogous to the conformational change in a lock washer. Thus, as the washer becomes flatter, the ends get closer. Correspondingly, we can measure a twisting motion of up to 12° around an axis lying along the extended head-to-head β-sheet. To aid in calculating and visualizing the mechanical motions in the UL44 dimer, a few specific "proxy" α-carbons were chosen whose positions span the various β-sheets (Fig. 5 and Table 2).

Peptide Binding Changes the Conformation of the Connector Loop—In the absence of bound peptide, the connector loop assumes a significantly different conformation (Fig. 6). The side chains of Gln^{51} and Leu^{60} serve as convenient reference points for understanding the change, as they are hydrogen-bonded to different main chain oxygen atoms of the connector loop in each of the two structures. With the UL54 peptide bound, these two side chains are hydrogen-bonded to the peptide oxygens of residues 134 and 136 (and the Ile^{135} side chain lies on the inward-facing surface of the two-stranded β-sheet and is buried). In contrast, in the crystal structure without the UL54 peptide, the main chain oxygens of residues 133 and 135 are hydrogen-bonded instead (and correspondingly, this middle portion of the connector loop, still in an extended conformation, is flipped over, exposing Ile^{135}) (Fig. 6*B*). To accommodate this one-residue translocation of the "middle" of the connector, the flanking loop sequence 129–132 must become more taut (in the peptide-free structure), whereas the flanking loop sequence 138–142 must loop outward to a greater extent. Note that these two flanking areas represent the regions of greatest localized conformational difference between the two crystal structures, with α-carbon shifts exceeding 6 Å.

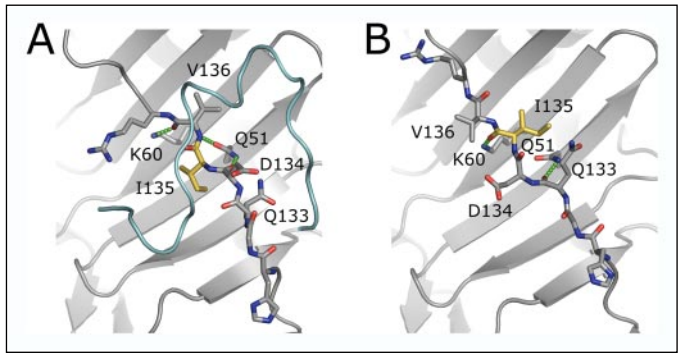

FIGURE 6. **The conformation of the connector loop differs in the crystal structures with peptide bound and without peptide.** *A*, in the presence of peptide, the connector loop is translated toward its N-terminal end, and the side chain of Ile^{135} (*yellow*) is buried. Hydrogen bonds between the connector loop and the peptide are omitted for clarity (see "Results and Discussion"). *B*, in the absence of peptide, the side chain of Ile^{135} is exposed and in a position similar to that of Val^{136} in the complex. Translation of the main chain causes the side chains of Lys^{60} and Gln^{51}, projecting upwards from the central β-sheet, to be hydrogen-bonded to different main chain oxygen atoms in the two cases.

The altered conformation is explained by the structure: when the peptide is bound, the position of the β-strand of the peptide is constrained by the position of its hydrophobic plug. In the complex, the register of the connector loop (Fig. 6*A*) is dictated by its ability to form the β-sheet hydrogen-bonding pattern with the peptide while simultaneously burying the side chains of Ile^{135} (Fig. 2*A*) and Val^{136} (Fig. 2*B*).

In the presence of the UL54 peptide, the connector loop forms many more specific interactions (Fig. 6). We therefore hypothesize that the binding of the UL54 peptide induces increased order in both the connector loop and the ligand. Indeed, such a dramatic increase in the number of interatomic contacts is consistent with tight binding of the peptide.

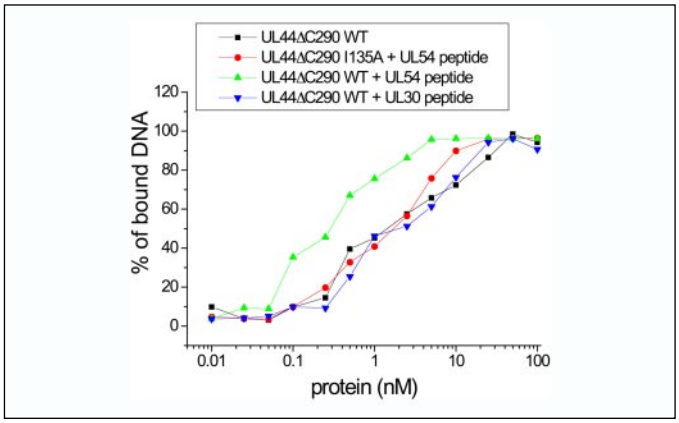

FIGURE 7. **Peptide-bound UL44 binds with higher affinity to DNA.** Increasing amounts of wild-type (*WT*) UL44ΔC290 were incubated with 1 fmol of radiolabeled double-stranded 30-bp DNA in the absence (*squares*) or presence of a peptide corresponding to the C-terminal 22 residues of HCMV UL54 (*triangles*) or to the C-terminal 36 residues of HSV UL30 (*inverted triangles*). As a control, increasing amounts of a mutant UL44 protein that does not bind UL54 (UL44ΔC290(I135A)) was also incubated in the presence of the UL54 C-terminal peptide (*circles*). Free and protein-bound DNAs were quantified by filter binding assays, and the fraction of protein-bound DNA is plotted against the protein concentration.

Peptide Binding Increases the Affinity of UL44 for DNA—We wished to rule out the possibility that opening and closing of the C-shaped clamp results from differences in crystal-packing interactions. Those changes that affect the back face of UL44 and the cavity of the homodimer would be predicted to affect the DNA binding properties of UL44. We therefore used a previously described filter binding assay (15) to compare the interaction of unliganded *versus* peptide-bound UL44ΔC290 with DNA (Fig. 7). Peptide-bound UL44ΔC290 exhibited a 4-fold lower apparent K_d for DNA than did unliganded UL44ΔC290. As a control, we also tested a UL44ΔC290 mutant (I135A) that does not detectably bind this peptide by isothermal titration calorimetry (19). In the presence of the UL54 peptide (Fig. 7) or its absence,[6] UL44ΔC290(I135A) bound DNA with the same affinity as wild-type UL44ΔC290 did in the absence of peptide. As an additional control, we tested a peptide corresponding to the C terminus of HSV UL30, and it did not affect the binding of wild-type UL44ΔC290 to DNA (Fig. 7). We conclude that the binding of the UL54 peptide to UL44 alters its conformation to increase its affinity for DNA.

The observed increase in affinity could be attributable to an increase in the on-rate, which might result from an opening of the binding site, and/or a decrease in the off-rate, which would be consistent with an improved complementarity between the protein and DNA in the complex. It should be noted, however, that the increased affinity of UL44 for DNA was observed under conditions in which two peptides bind per UL44 dimer. It is not clear whether both monomers would be occupied in a UL44-UL54 complex *in vivo*, or if binding a single peptide would be sufficient to propagate the change to the other monomer in the dimer pair. Regardless, these results suggest that conformational changes in UL44 upon UL54 binding may play a biological role in regulating the affinity of the dimer for duplex DNA. One simple possibility is that the conformational change simply increases affinity, thereby promoting processivity. An alternative possibility is that one conformation of UL44 might be shaped to bind classic B-form DNA better in the absence of UL54. During DNA replication, however, UL44 may have to adapt to DNA that is less like the classic B-form due to distortions caused by the HCMV DNA polymerase during translocation on the DNA template.

[6] A. Loregian and D. M. Coen, unpublished data.

UL44 May Be Capable of Forming Higher Order Aggregates—The crystal structure of the complex with the peptide also points out a way that UL44 might form higher order aggregates when bound to DNA. Thus, in the crystal structure of the complex with the peptide, crystal packing either creates or stabilizes a second 2-fold interface. This additional interface involves extended β-interactions between the four-stranded β-sheets at the C-terminal end of the molecules (tail end), rather than the five-stranded β-sheets at the N-terminal ends (head end). With both interfaces forming extended β-sheets, a continuous helical arrangement of C clamp-shaped dimers is created in the crystal with the peptide bound, having an inner diameter of ~45 Å. This second interface appears to be significantly weaker than the head-to-head interaction, as it lacks the intricate interdigitation of aromatic and aliphatic side chains that stabilizes the latter (15); it buries approximately three-fourths as much total surface area (see Table 2); shape complementarity is less (Table 2); and no higher order aggregates are detected in solution (15). Nevertheless, the second dimer interface still exhibits a greater degree of structural complementarity than what is usually required for a macromolecular crystal-packing contact.

A recent electron microscopy study indicated that the UL44 homolog from the γ-herpesvirus Epstein-Barr virus assembles in a higher ordered structure that is reminiscent of a lock washer or ring-like arrangement (60). Furthermore, the inner diameter of the rings in these electron microscope images have widths similar to that of the central cavity of the infinite "lock washer" helical arrangement of dimers observed in the UL44-UL54 crystal lattice. Although the putative biological function of these higher order assemblies is unknown, UL44 and other herpesvirus processivity factors are present in excess relative to their catalytic subunits, and these "spare" subunits may be associated with DNA. Therefore, future studies should keep in mind that, when multiple copies of the C clamp-shaped dimer are bound to the same DNA duplex or in the vicinity of the same replication fork, they may have a tendency to associate along the weaker interface and form higher ordered complexes as a result.

Acknowledgments—We thank Doryen Bubeck, Brandt Eichman, John Randell, Eric Toth, and Harmon Zuccola for helpful discussions; Chuck Dahl for peptide synthesis; Laura Guogas for help with data collection; Daniel Floyd for help with crystallization experiments; and Stephan Ginell and the staff of the Advanced Photon Source for technical assistance.

REFERENCES

1. Jeruzalmi, D., O'Donnell, M., and Kuriyan, J. (2002) *Curr. Opin. Struct. Biol.* **12,** 217–224
2. Wu, C. A., Nelson, N. J., McGeoch, D. J., and Challberg, M. D. (1988) *J. Virol.* **62,** 435–443
3. Pari, G. S., and Anders, D. G. (1993) *J. Virol.* **67,** 6979–6988
4. Pari, G. S., Kacica, M. A., and Anders, D. G. (1993) *J. Virol.* **67,** 2575–2582
5. Heilbronn, R., Jahn, G., Burkle, A., Freese, U. K., Fleckenstein, B., and zur Hausen, H. (1987) *J. Virol.* **61,** 119–124
6. Kouzarides, T., Bankier, A. T., Satchwell, S. C., Weston, K., Tomlinson, P., and Barrell, B. G. (1987) *J. Virol.* **61,** 125–133
7. Ertl, P. F., and Powell, K. L. (1992) *J. Virol.* **66,** 4126–4133
8. Cihlar, T., Fuller, M. D., and Cherrington, J. M. (1997) *Protein Expression Purif.* **11,** 209–218
9. Mar, E. C., Chiou, J. F., Cheng, Y. C., and Huang, E. S. (1985) *J. Virol.* **56,** 846–851
10. Nishiyama, Y., Maeno, K., and Yoshida, S. (1983) *Virology* **124,** 221–231
11. Gottlieb, J., Marcy, A. I., Coen, D. M., and Challberg, M. D. (1990) *J. Virol.* **64,** 5976–5987
12. Loregian, A., Appleton, B. A., Hogle, J. M., and Coen, D. M. (2004) *J. Virol.* **78,** 158–167
13. Weiland, K. L., Oien, N. L., Homa, F., and Wathen, M. W. (1994) *Virus Res.* **34,** 191–206
14. Gibson, W., Murphy, T. L., and Roby, C. (1981) *Virology* **111,** 251–262
15. Appleton, B. A., Loregian, A., Filman, D. J., Coen, D. M., and Hogle, J. M. (2004) *Mol.*

Cell **15,** 233–244
16. Zuccola, H. J., Filman, D. J., Coen, D. M., and Hogle, J. M. (2000) *Mol. Cell* **5,** 267–278
17. Gulbis, J. M., Kelman, Z., Hurwitz, J., O'Donnell, M., and Kuriyan, J. (1996) *Cell* **87,** 297–306
18. Krishna, T. S., Kong, X. P., Gary, S., Burgers, P. M., and Kuriyan, J. (1994) *Cell* **79,** 1233–1243
19. Loregian, A., Appleton, B. A., Hogle, J. M., and Coen, D. M. (2004) *J. Virol.* **78,** 9084–9092
20. Thornton, K. E., Chaudhuri, M., Monahan, S. J., Grinstead, L. A., and Parris, D. S. (2000) *Virology* **275,** 373–390
21. Weisshart, K., Chow, C. S., and Coen, D. M. (1999) *J. Virol.* **73,** 55–66
22. Parris, D. S., Cross, A., Haarr, L., Orr, A., Frame, M. C., Murphy, M., McGeoch, D. J., and Marsden, H. S. (1988) *J. Virol.* **62,** 818–825
23. Gottlieb, J., and Challberg, M. D. (1994) *J. Virol.* **68,** 4937–4945
24. Chen, X., Lin, K., and Ricciardi, R. P. (2004) *J. Biol. Chem.* **279,** 28375–28386
25. Randell, J. C., and Coen, D. M. (2004) *J. Mol. Biol.* **335,** 409–413
26. Crute, J. J., and Lehman, I. R. (1989) *J. Biol. Chem.* **264,** 19266–19270
27. Gallo, M. L., Jackwood, D. H., Murphy, M., Marsden, H. S., and Parris, D. S. (1988) *J. Virol.* **62,** 2874–2883
28. Digard, P., Bebrin, W. R., Weisshart, K., and Coen, D. M. (1993) *J. Virol.* **67,** 398–406
29. Loregian, A., Rigatti, R., Murphy, M., Schievano, E., Palu, G., and Marsden, H. S. (2003) *J. Virol.* **77,** 8336–8344
30. Bridges, K. G., Hua, Q., Brigham-Burke, M. R., Martin, J. D., Hensley, P., Dahl, C. E., Digard, P., Weiss, M. A., and Coen, D. M. (2000) *J. Biol. Chem.* **275,** 472–478
31. Bridges, K. G., Chow, C. S., and Coen, D. M. (2001) *J. Virol.* **75,** 4990–4998
32. Otwinowski, Z., and Minor, W. (1997) *Methods Enzymol.* **276,** 307–326
33. Terwilliger, T. C., and Berendzen, J. (1999) *Acta Crystallogr. Sect. D Biol. Crystallogr.* **55,** 849–861
34. Terwilliger, T. C. (2000) *Acta Crystallogr. Sect. D Biol. Crystallogr.* **56,** 965–972
35. McRee, D. E. (1999) *J. Struct. Biol.* **125,** 156–165
36. Murshudov, G. N., Vagin, A. A., and Dodson, E. J. (1997) *Acta Crystallogr. Sect. D Biol. Crystallogr.* **53,** 240–255
37. Laskowski, R. A., MacAurthur, M. W., Moss, D. S., and Thornton, J. M. (1993) *J. Appl. Crystallogr.* **26,** 283–291
38. Kraulis, P. J. (1991) *J. Appl. Crystallogr.* **24,** 946–950
39. Merritt, E. A., and Bacon, D. J. (1997) *Methods Enzymol.* **277,** 505–524
40. Lawrence, M. C., and Colman, P. M. (1993) *J. Mol. Biol.* **234,** 946–950
41. Vivona, J. B., and Kelman, Z. (2003) *FEBS Lett.* **546,** 167–172
42. Maga, G., and Hubscher, U. (2003) *J. Cell Sci.* **116,** 3051–3060
43. Chapados, B. R., Hosfield, D. J., Han, S., Qiu, J., Yelent, B., Shen, B., and Tainer, J. A. (2004) *Cell* **116,** 39–50
44. Bruning, J. B., and Shamoo, Y. (2004) *Structure* (*Camb.*) **12,** 2209–2219
45. Sakurai, S., Kitano, K., Yamaguchi, H., Hamada, K., Okada, K., Fukuda, K., Uchida, M., Ohtsuka, E., Morioka, H., and Hakoshima, T. (2005) *EMBO J.* **24,** 683–693
46. Matsumiya, S., Ishino, S., Ishino, Y., and Morikawa, K. (2002) *Genes Cells* **7,** 911–922
47. Bowman, G. D., O'Donnell, M., and Kuriyan, J. (2004) *Nature* **429,** 724–730
48. Shamoo, Y., and Steitz, T. A. (1999) *Cell* **99,** 155–166
49. Kong, X. P., Onrust, R., O'Donnell, M., and Kuriyan, J. (1992) *Cell* **69,** 425–437
50. Jeruzalmi, D., Yurieva, O., Zhao, Y., Young, M., Stewart, J., Hingorani, M., O'Donnell, M., and Kuriyan, J. (2001) *Cell* **106,** 417–428
51. Bunting, K. A., Roe, S. M., and Pearl, L. H. (2003) *EMBO J.* **22,** 5883–5892
52. Burnouf, D. Y., Olieric, V., Wagner, J., Fujii, S., Reinbolt, J., Fuchs, R. P., and Dumas, P. (2004) *J. Mol. Biol.* **335,** 1187–1197
53. Pages, V., and Fuchs, R. P. (2002) *Oncogene* **21,** 8957–8966
54. Coen, D. M., and Schaffer, P. A. (2003) *Nat. Rev. Drug Discov.* **2,** 278–288
55. Ripalti, A., Boccuni, M. C., Campanini, F., and Landini, M. P. (1995) *J. Virol.* **69,** 2047–2057
56. Digard, P., Williams, K. P., Hensley, P., Brooks, I. S., Dahl, C. E., and Coen, D. M. (1995) *Proc. Natl. Acad. Sci. U. S. A.* **92,** 1456–1460
57. Pilger, B. D., Cui, C., and Coen, D. M. (2004) *Chem. Biol.* **11,** 647–654
58. Loregian, A., and Coen, D. M. (2006) *Chem. Biol.*, in press
59. Hayward, S., and Berendsen, H. J. (1998) *Proteins* **30,** 144–154
60. Makhov, A. M., Subramanian, D., Holley-Guthrie, E., Kenney, S. C., and Griffith, J. D. (2004) *J. Biol. Chem.* **279,** 40358–40361

Crystal Structure of the Cytomegalovirus DNA Polymerase Subunit UL44 in Complex with the C Terminus from the Catalytic Subunit: DIFFERENCES IN STRUCTURE AND FUNCTION RELATIVE TO UNLIGANDED UL44

Brent A. Appleton, Justin Brooks, Arianna Loregian, David J. Filman, Donald M. Coen and James M. Hogle

J. Biol. Chem. 2006, 281:5224-5232.
doi: 10.1074/jbc.M506900200 originally published online December 20, 2005
